MPMI Vol. 37, No. 2, 2024, pp. 112–126, https://doi.org/10.1094/MPMI-04-23-0051-R

Additive and Specific Effects of Elicitor Treatments on the Metabolic Profile of *Arabidopsis thaliana*

Lisa Cabre,[1] Lun Jing,[2] Moffat Makechemu,[3] Kylhan Heluin,[4] Sarah El Khamlichi,[4] Jérôme Leprince,[5] Marie Christine Kiefer-Meyer,[4] Sylvain Pluchon,[1] Jean-Claude Mollet,[4] Cyril Zipfel,[3,6] and Eric Nguema-Ona[1,†]

[1] Centre Mondial de l'Innovation–Groupe Roullier (CMI-Roullier), Laboratoire de Nutrition Végétale, Saint Malo, F-35400, France
[2] Centre Mondial de l'Innovation–Groupe Roullier (CMI-Roullier), Plateforme de Chimie et Bio-Analyse, Saint Malo, F-35400, France
[3] Department of Plant and Microbial Biology, Zurich-Basel Plant Science Center, University of Zürich, CH-8008 Zürich, Switzerland
[4] Université de Rouen Normandie, GLYCOMEV UR 4358, SFR Normandie Végétal FED 4277, Innovation Chimie Carnot, RMT BESTIM, GDR Chémobiologie, IRIB, F-76000 Rouen, France
[5] Université de Rouen Normandie, CNRS, INSERM, HERACLES US 51 UAR 2026, PRIMACEN, IRIB, F-76000 Rouen, France
[6] The Sainsbury Laboratory, University of East Anglia, Norwich Research Park, NR4 7UH Norwich, U.K.

Accepted for publication 26 October 2023.

Several elicitors of plant defense have been identified and numerous efforts to use them in the field have been made. Exogenous elicitor treatments mimic the in planta activation of pattern-triggered immunity (PTI), which relies on the perception of pathogen-associated molecular patterns (PAMPs) such as bacterial flg22 or fungal chitins. Early transcriptional responses to distinct PAMPs are mostly overlapping, regardless of the elicitor being used. However, it remains poorly known if the same patterns are observed for metabolites and proteins produced later during PTI. In addition, little is known about the impact of a combination of elicitors on PTI and the level of induced resistance to pathogens. Here, we monitored *Arabidopsis thaliana* resistance to the bacterial pathogen *Pseudomonas syringae* pv. *tomato* DC3000 (*Pto* DC3000) following application of flg22 and chitosan elicitors, used individually or in combination. A slight, but not statistically significant increase in induced resistance was observed when the elicitors were applied together when compared with individual treatments. We investigated the effect of these treatments on the metabolome by using an untargeted analysis. We found that the combination of flg22 and chitosan impacted a higher number of metabolites and deregulated specific metabolic pathways compared with the elicitors individually. These results contribute to a better understanding of plant responses to elicitors, which might help better rationalize their use in the field.

Keywords: *Arabidopsis thaliana*, elicitors, metabolomics, plant defense, plant protection

Plants have the potential to manage threats caused by pathogens and pests. Indeed, they are equipped with an innate, inducible immune system, which can protect them against most microbes (Jones and Dangl 2006). The plant immune system consists of two lines of perception against pathogens and pests. The first one involves cell-surface pattern recognition receptors able to recognize pathogen/pest-associated molecular patterns (PAMPs), leading to pattern-triggered immunity (PTI) (Boller and Felix 2009; Chisholm et al. 2006). The second utilizes cytosolic nucleotide-binding site leucine-rich repeat receptors able to recognize pathogen/pest virulence effectors activating effector-triggered immunity (ETI) (Ngou et al. 2022). Understanding and harnessing plant immunity have translated into several biotechnological approaches, all aimed at protecting crops against bio-aggressors. These approaches encompass breeding and engineering for crop cultivars tolerant/resistant to pathogen/pests, including the exploitation of plant pattern recognition receptors (PRRs) (Boutrot and Zipfel 2017), genome-editing of susceptibility genes (Langner et al. 2018), or the application of plant elicitors (PEs) to activate PTI (Boller and Felix 2009). PEs are either PAMPs, such as the bacterial flagellin-derived flg22 peptide (Felix et al. 1999) or fungal chitin-derived (Felix et al. 1993; Shibuya et al. 1993; Yamada et al. 1993) or chitosan-derived (Jia et al. 2018) oligosaccharides; damage-associated molecular patterns (Hahn et al. 1981; Hou et al. 2019); phytocytokines (Gust et al. 2017); or plant- or animal-derived

[†]Corresponding author: E. Nguema-Ona; eric.nguemaona@roullier.com

Author contributions: E.N.-O. conceived the project, conceived the initial experimental design, and wrote the manuscript with contribution from all authors. E.N.-O. and L.C. wrote the first draft of the manuscript. E.N.-O., L.C., L.J., M.M., M.C.K.-M., S.P., J.-C.M., and C.Z. provided feedback on the manuscript. L.C., L.J., M.M., M.C.K.-M., J.-C.M., and C.Z. contributed to further experimental design. E.N.-O., L.C., L.J., M.M., and M.C.K.-M. designed the experiments and analyzed the data. K.H., S.E.K., and M.M. performed most of the experiments. E.N.-O., J.L., J.-C.M., S.P., and C.Z. contributed reagents/analytical tools.

Funding: Funding was provided by the Schweizerischer Nationalfonds zur Förderung der Wissenschaftlichen Forschung (189340) to C. Zipfel.

e-Xtra: Supplementary material is available online.

The author(s) declare no conflict of interest.

exogenous substances (Klarzynski et al. 2000; Přerovská et al. 2022). Induced resistance (IR) following the activation of PTI has received renewed attention, as it has the potential to be integrated into pest management (Sandroni et al. 2020). In addition, PTI is commonly assumed to be more durable than ETI (Mundt 2014), although it is known that pathogen effectors may target components of PTI (Wang et al. 2022). The activation of PTI can be sequenced into early and late events, which ultimately lead to IR against plant pests and pathogens (Yu et al. 2017).

The model plant *Arabidopsis thaliana* L. (Heynh.) (hereafter *Arabidopsis*) has been particularly useful in identifying PEs and corresponding PRRs. Plant PRRs are transmembrane receptors that contain an extracellular domain able to recognize and bind PEs in a specific manner and that do or do not contain a cytosolic kinase (receptor kinases [RKs] or receptor proteins, respectively) (DeFalco and Zipfel 2021). Upon PE binding, PRRs form multiprotein complexes, leading to PTI activation (DeFalco and Zipfel 2021; Yu et al. 2017). For instance, *At*FLS2 (FLAGELLIN-SENSING 2) is a leucine-rich repeat-RK that recognizes flg22 (Gómez-Gómez and Boller 2000). Upon flg22 binding, *At*FLS2 forms a complex with the co-receptor *At*BRASSINOSTEROID-INSENSITIVE1 (BRI1)-ASSOCIATED RECEPTOR KINASE 1 (*At*BAK1) or *At*BAK1-LIKE KINASE 1 (*At*BKK1), to activate PTI signaling (Chinchilla et al. 2007; Heese et al. 2007; Roux et al. 2011; Schwessinger et al. 2011; Sun et al. 2013). Fungal-derived chitin and/or chitosan oligomers are perceived by a complex containing the LysM-RKs *At*LYK5 as main ligand-binding receptor and *At*CERK1 (CHITIN ELICITOR RECEPTOR KINASE1) as a co-receptor (Cao et al. 2014; Gubaeva et al. 2018; Liu et al. 2012; Miya et al. 2007; Wan et al. 2008).

Late PTI signaling events include the synthesis of callose deposits (Luna et al. 2011), the synthesis and secretion of pathogenesis-related proteins (van Loon et al. 2006), as well as nonprotein antimicrobial compounds (Zaynab et al. 2018). Antimicrobial phytoalexins encompass a large group of defense-inducible, specialized secondary metabolites, including phenolics, terpenoids, glycoalkaloids, and glucosinolates (Ahuja et al. 2012). Often defined as end products of plant secondary metabolisms, phytoalexins are associated with late PTI events (Ahuja et al. 2012; Piasecka et al. 2015). However, the general function assigned to accumulating secondary metabolites, including PTI inducible-phytoalexins, is progressively extending toward additional roles as indirect suppliers of primary metabolites to plants (Erb and Kliebenstein 2020).

Important efforts in understanding PTI activation followed by an effective production of resistance metabolites and proteins have been accomplished during the last 20 years (DeFalco and Zipfel 2021; Ngou et al. 2022; Yu et al. 2017). Focusing on early (minutes to hours) events accompanying PTI activation, Bjornson et al. (2021) observed common transcriptional trends after the application of various PEs in Arabidopsis. The congruence of the response was irrespective of the PRR-PE pairs being tested and confirmed previous observations (Wan et al. 2008; Zipfel et al. 2006). However, whether this congruence is also reflected in the production of defense metabolites and proteins, which takes place during the later stages of PTI, remains to be tested. Another question to answer is how plants respond to multiple stimulations by PEs. Indeed, it is relevant to study the response to multiple PEs rather than individual ones, as plants naturally exposed to potential pathogens can recognize in principle several PEs from an organism (e.g., flagellin and EF-Tu from bacteria) or from a variety of organisms (e.g., flagellin from bacteria and chitin from fungi; DeFalco and Zipfel 2021) present at the plant surface. In addition, bio-based extracts that contain several potential PEs are increasingly used in agriculture, and thus it is important to understand the combined responses to multiple PEs (de Borba et al. 2021; Martin et al. 2020; Přerovská et al. 2022).

Here, we first monitored *Arabidopsis* resistance to infection caused by *Pseudomonas syringae* pv. *tomato* DC3000 (*Pto* DC3000) following application of two well-characterized pathogen-associated molecular pattern-plant elicitors (PAMP-PEs), flg22 and chitosan oligosaccharides, used individually or in combination. Both these PEs bind to two different PRRs (FLS2 for flg22 and LYK5 for chitin/chitosan), engaging different co-receptors (BAK1 for FLS2, CERK1 for chitin/chitosan), and they represent prototypical PAMPs present in microbes widely present on leaf surfaces (bacteria for flagellin, fungi for chitin/chitosan). In addition, the ability of these PRRs to perceive flg22 and chitin/chitosan is conserved in Angiosperms, which include the vast majority of crops.

To test whether the congruence observed during early PTI events also results in similar observations during the late events, we performed untargeted metabolite profiling on *Arabidopsis* at 24 h and 48 h after application of flg22, chitosan, or both at different concentrations.

Results

Flg22 and chitosan, alone or in combination, induced antibacterial resistance in a manner dependent on their respective receptors and co-receptors

To validate the effective induction of the PTI in our experimental conditions, we monitored the induction of PTI biomarkers. Thirty minutes after application of PE, flg22, or chitosan, the plantlets were collected, and we monitored the accumulation of reactive oxygen species (ROS) using nitro blue tetrazolium chloride (NBT) staining when compared with control plants; both treatments induced ROS accumulation (Supplementary Fig. S1A and B). The presence of callose deposits following the applications of both PEs was also monitored using aniline blue staining. Both treatments resulted in callose deposition in *Arabidopsis* plantlets (Supplementary Fig. S1C). These results indicated that individually, both the treatments led to an activation of PTI, as previously reported (Bjornson et al. 2021; Ye et al. 2020).

Then, we measured the level of IR against the bacterium *Pseudomonas syringae* pv. *tomato* DC3000 (*Pto* DC3000) on *Arabidopsis* plants following the application of flg22, chitosan, or a combination of both PEs. As expected, when pretreated with flg22 or chitosan, *Pto* DC3000 titers were reduced in infiltrated wild-type (WT) *Arabidopsis* leaves compared with mock-treated (control) plants (Fig. 1A). This supported the activation of PTI in our experimental conditions (Supplementary Fig. S1) and confirmed existing data on flg22 and chitosan (Jia et al. 2018; Zipfel et al. 2004). Notably, the measured IR was dependent on known receptors or co-receptors for flg22 and chitosan (Gómez-Gómez and Boller 2000; Miya et al. 2007; Wan et al. 2008; Fig. 1). Interestingly, when flg22 and chitosan were combined, *Pto* DC3000-infiltrated WT *Arabidopsis* leaves exhibited a small increase of IR, when compared with individual flg22 or chitosan treatments, although this was not statistically significant. However, the measured IR did not indicate a cumulative or additive effect (Fig. 1A). We also evaluated the effects of suboptimal concentrations of PE applied individually (10 nM and 100 nM for flg22; 0.01 mg/ml and 0.1 mg/ml for chitosan) or in combination (10 nM flg22 + 0.01 mg/ml chitosan; 100 nM flg22 + 0.1 mg/ml chitosan) on *Arabidopsis* IR to *Pto* DC3000 (Supplementary Fig. S2) and ROS production (Supplementary Fig. S3). We observed a decrease in *Pto* DC3000 titers when each PE was applied individually at suboptimal elicitor concentrations, indicating a gradual, dose-dependent increase in IR (Supplementary Fig. S2). When both PEs were applied at

suboptimal concentrations, an increase in IR was visible. However, this increase was not additive, based on the statistical tests performed (Supplementary Fig. S2). We also observed a gradual, dose-dependent increase in ROS production when each PE was applied individually at both suboptimal PE concentrations (Supplementary Fig. S3). However, when both PEs were applied at suboptimal concentrations, we did observe an additive effect on ROS production, but not a synergistic effect (Supplementary Fig. S3).

Simultaneous flg22 and chitosan treatment did not overactivate biological markers of PTI activation

It has been shown that distinct PEs activate common transcriptional changes in early stages of PTI (Bjornson et al. 2021). Here, we investigated how a simultaneous application of flg22 and chitosan impacts PTI transcriptional and metabolic responses at early (3 h) and late (24 to 48 h) time points. Flg22-, chitosan-, and flg22 + chitosan-treated 10-day-old *Arabidopsis* plantlets were analyzed for their salicylic acid (SA) content at 24 h and 48 h posttreatment (Fig. 2A). As expected (Jia et al. 2018; Tsuda et al. 2008), an increase in SA content was observed in both flg22- and chitosan-treated plantlets, particularly at 24 h after treatment, when compared with untreated WT plants. At 48 h after treatment, we could still measure an increase in SA content following an individual application of PE, but with a lowered amplitude (Fig. 2A). The combination flg22 + chitosan also yielded an increase in SA content at 24 h after the treatment when compared with untreated WT plants but did not produce more SA than individual treatment. After 48 h of treatment, SA content was similar to the level measured in flg22-treated plantlets (Fig. 2A). This reduced SA content could possibly reflect saturation of the downstream signaling components, suggesting that upon a combined application of PEs, plants would respond differentially. While able to bind their cognate ligand, co-RK mutants are altered in their ability to transduce PTI signal. The *bak1-5 bkk1* double mutant is unable to mediate the intracellular activation of PTI following flg22 perception, and the *cerk1* mutant is unable to mediate the corresponding intracellular activation of PTI following chitin/chitosan perception (Miya et al. 2007; Roux et al. 2011; Schwessinger et al. 2011; Wan et al. 2008). The *bak1-5 bkk1 cerk1* (*bbc*) triple mutant (Xin et al. 2016) is therefore unable to relay the perception of both flg22 and chitosan. Ten-day-old *Arabidopsis* co-RK mutant treated plantlets were also analyzed for their SA content at 24 h after treatment (Fig. 2B). The *bbc* mutant did not respond to any of the treatments, as SA content did not change (Fig. 2B). As expected, the single and double mutant controls responded differently to the different treatments. When treated with their cognate ligand, *bak1-5 bkk1* and *cerk1* exhibited poor SA yield. The *bak1-5 bkk1* double mutant responded to chitosan stimulation, whereas the *cerk1* single mutant respond to flg22 treatment. This showed that SA accumulation is dependent on corresponding co-RKs for the PEs tested, as expected. We also evaluated the effects of suboptimal concentrations of PEs on SA accumulation, when applied individually (10 nM and 100 nM for flg22; 0.01 mg/ml and 0.1 mg/ml for chitosan) or in combination (10 nM flg22 + 0.01 mg/ml chitosan; 100 nM flg22 + 0.1 mg/ml chitosan) (Supplementary Fig. S4). Note that tested concentrations yielded a much lower amount of SA. Nevertheless, we compared SA accumulation in these experimental conditions. We did not observe a gradual, dose-dependent increase in SA accumulation when both PEs were applied individually (Supplementary Fig. S4). We did observe an additive effect on SA content only with the 100 nM flg22 + 0.1 mg/ml chitosan treatment when applied in combination (Supplementary Fig. S4). We also monitored the level of expression of the gene *WRKY29* encoding a transcription factor, another biomarker of early PTI events (Asai et al. 2002). Ten-day-old *Arabidopsis* plantlets were treated, and the time course of *WRKY29* transcript accumulation upon PE treatments was followed (Fig. 2C). As expected, flg22 and chitosan treatment increased *WRKY29* transcript levels in WT, particularly after 3 h, in a manner that was dependent on corresponding co-RKs (Fig. 2C and D). Flg22 + chitosan treatment induced *WRKY29* transcript levels similar to those observed after flg22 treatment alone (Fig. 2C), possibly reflecting a saturation of the downstream signaling components. Later, the synthesis of *WRKY29* transcripts decreased (Fig. 2C), illustrating the possible role of this transcription factor during early events of PTI activation. We also measured transcript levels of other early marker PTI genes such as *RBOHD* (*RESPIRATORY BURST OXIDASE HOMOLOGUE D*) (Nühse et al. 2007) and *PAD3* (*PHYTOALEXIN DEFICIENT 3*) (Thomma et al. 1999). Upon the PE treatments

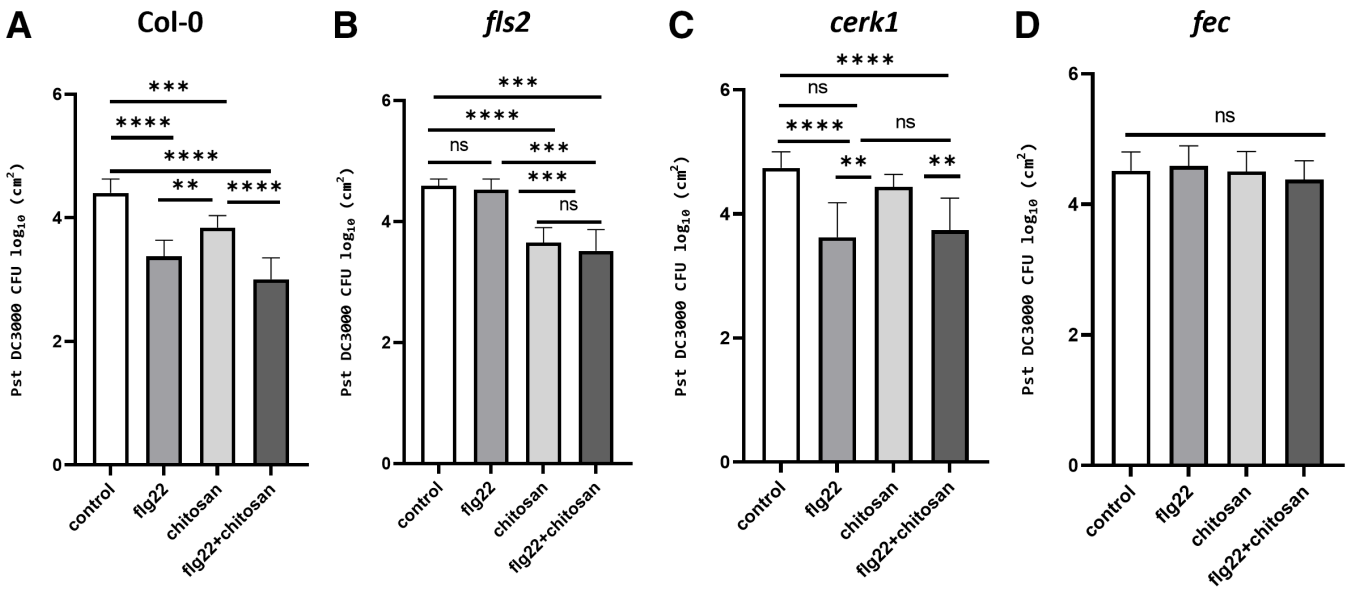

Fig. 1. Effect of one or a combination of plant elicitors (PEs) on *Arabidopsis thaliana* induced resistance against *Pseudomonas syringae*. **A,** Col-0, **B,** *fls2*, **C,** *cerk1*, or **D,** *fls2 efr cerk1* (*fec*) seedlings were inoculated at 24 h after elicitation. At 48 h postinoculation, bacterial growth (CFU, colony-forming unit) was measured. Mean ± SD of three biological replicates. The number of plantlets per biological replicate was $n = 12$ for all genotype–treatment combinations, per biological repetition. Asterisks (*) indicate a significant difference (one-way ANOVA): $^{**}P < 0.01$; $^{***}P < 0.001$; $^{****}P < 0.0001$; ns, not significant.

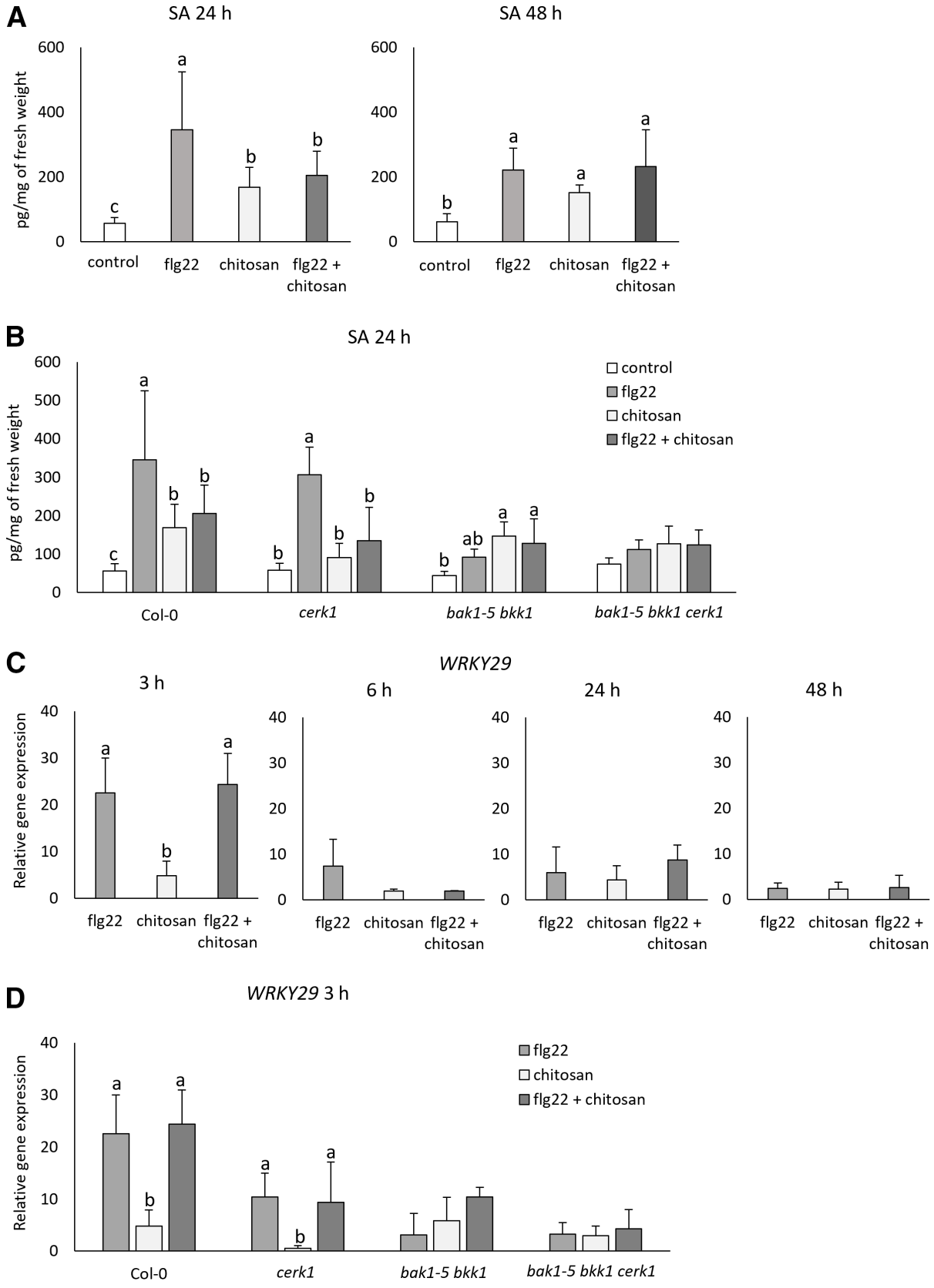

Fig. 2. Impact of one or a combination of plant elicitors (PEs) on pattern-triggered immunity (PTI) markers. **A,** Salicylic acid (SA) quantification after 24 and 48 h of elicitation. The number of plantlets per biological replicate experiment was $n = 15$ plants for all genotype–treatment combinations, per biological repetition. Mean ± SD of four to six biological replicates. **B,** SA quantification in wild-type (WT, Col-0) and mutant (*cerk1*, *bak1-5 bkk1*, and *bak1-5 bkk1 cerk1*) seedlings at 24 h post-elicitation. Mean ± SD of five replicates. **C**, Impact of the different elicitors on *WRKY29* (AT4G23550) expression in WT plants after 3, 6, 24, and 48 h. **D,** *WRKY29* expression at 3 h posttreatment in WT (Col-0) and mutant (*cerk1*, *bak1-5 bkk1*, and *bak1-5 bkk1 cerk1*) seedlings. RT-qPCR analysis was carried out to quantify transcript accumulation compared with the control plants. The *ROC3* gene (AT2G16600) was used as a reference (Kanno et al. 2016). Three independent biological replicates ± SE. Different letters indicate a significant difference based on analysis of variance followed by the Student–Newman–Keuls test ($P < 0.05$).

described above, changes in *RBOHD* and *PAD3* transcript levels behaved comparably to those seen for *WRKY29* (Supplementary Fig. S5).

Application of flg22, chitosan, or their combination led to contrasting metabolite patterns

To study *Arabidopsis* responses to flg22 as well as to chitosan application at 24 h after treatment, we undertook an untargeted profiling of the whole metabolome of WT *Arabidopsis*. This approach (i) offers the possibility to monitor biochemical markers associated with late PTI events, with a focus on biochemical pathways leading to the production of phytoalexin-related antimicrobial compounds; (ii) and also offers the possibility to apprehend additional visible trends when the entire metabolome is monitored and can thus help our understanding of late PTI events. To this end, 10-day-old WT *Arabidopsis* plantlets were treated with flg22, chitosan, or flg22 + chitosan; sampled at 24 h posttreatment; and then analyzed using ultra-performance liquid chromatography–tandem mass spectrometry (UPLC-MS/MS) (Schläpfer et al. 2017). We identified a set of metabolites using the Plant Metabolic Network database (https://plantcyc.org; see also Chae et al. 2014; Schläpfer et al. 2017), which covers pathways of secondary metabolism, including phytoalexin-related metabolites and primary metabolites such as amino acids, organic acids, lipids, sugars, and purines (Supplementary Table S1). Treated plants showed PE-dependent deregulated compounds (univariate statistical analysis, cutoff of P value < 0.05 and fold change > 2 or < 0.5). Compared with the control, 174 deregulated compounds were identified in positive ionization mode and 108 in negative ionization mode after flg22 treatment. In chitosan-treated samples, 108 and 83 features were identified in positive and negative ionization modes, respectively. Following flg22 + chitosan treatments, 237 impacted features were identified under positive ionization mode and 157 under negative ionization mode (Fig. 3A). The deregulated compounds identified under positive and negative ionization were pooled. For the metabolites identified under both ionization modes, only the data related to the ionization mode, in which the normalized abundance was the highest, were considered. Totals of 242, 175, and 330 metabolites were differentially regulated in flg22-, chitosan-, and flg22 + chitosan-treated plantlets, respectively (Fig. 3B; Supplementary Table S1). We observed that each group produced treatment-specific metabolites (Fig. 3B). Flg22-treated plants were enriched with 23% of secondary metabolites, and chitosan-treated plants with 31% (Supplementary Table S1). When treated simultaneously with

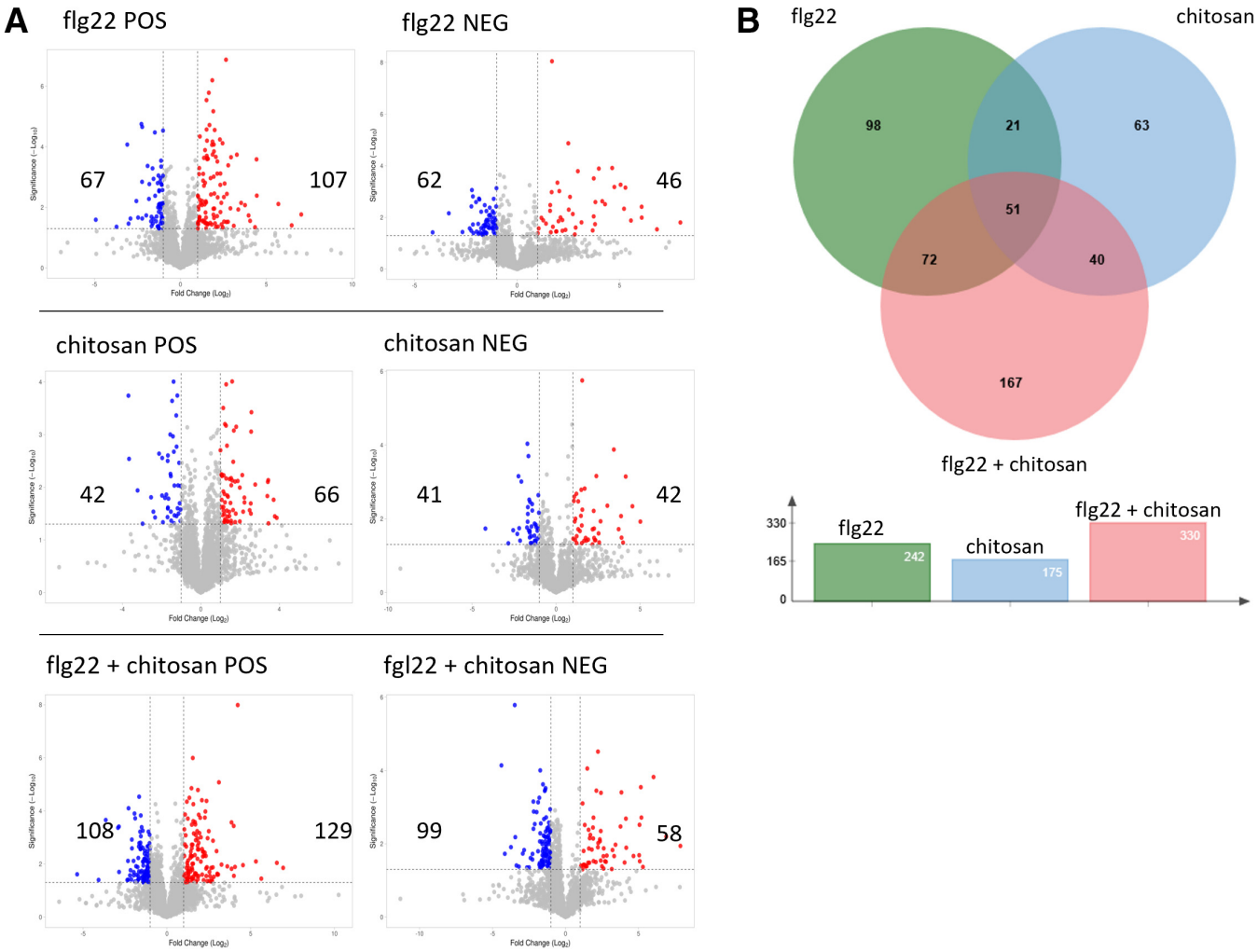

Fig. 3. Differential metabolic response after flg22, chitosan, or flg22 + chitosan treatments. **A,** Volcano plots of the metabolites identified under positive (POS) and negative (NEG) ionization modes. The colors indicate the metabolites accumulated differentially under the cutoff of P value < 0.05 and fold changes > 2 or < 0.5. The number of deregulated metabolites identified in each condition is indicated. **B,** Common and specific deregulated metabolites following *Arabidopsis thaliana* seedling elicitation. Venn diagram of the differentially accumulated metabolites after the different treatments (cutoff P value < 0.05 and fold changes > 2 or < 0.5). The number of significantly deregulated metabolites identified in each treatment is shown under the diagram.

flg22 and chitosan, 32% of the deregulated metabolites were annotated as secondary metabolites (Supplementary Table S1). We also noticed that a simultaneous application of flg22 and chitosan yielded more differentially regulated metabolites than a single PE application (Fig. 3A and B). Only 51 metabolites were common to all the treatments, and 21 metabolites were common to flg22-treated and chitosan-treated plantlets (Fig. 3B). We then focused on phytoalexin-related metabolites deregulated by each treatment, as they encompass a large group of PTI-inducible secondary metabolites, including phenolic compounds, glycoalkaloids, glucosinolates, and terpenoids (Ahuja et al. 2012). Flg22-treated plants yielded 58 phytoalexin-related compounds (20 phenolics, 15 flavonoids, 17 alkaloids, 5 terpenoids, and 1 glucosinolate), chitosan-treated plants yielded 55 phytoalexin-related compounds (23 phenolics, 12 flavonoids, 18 alkaloids, and 2 terpenoids), and simultaneous application of both Pes impacted 106 phytoalexin-related compounds (44 phenolics, 21 flavonoids, 31 alkaloids, 8 terpenoids, and 2 glucosinolates). Considering the deregulation of many phenylpropanoids (Fig. 4A), we looked in more detail at how the flg22 + chitosan treatment impacted the phenylpropanoid biosynthesis pathways (Fig. 4B). The pathway leading to coniferin and syringin synthesis appeared to be downregulated, whereas flavonoid biosynthesis was activated. The combined application of flg22 + chitosan led to the specific accumulation of sinapine, naringin, fisetin, and xanthohumol. All metabolomic changes measured were dependent on relevant co-RKs for the respective PEs, as no metabolic pathways were found to be deregulated after flg22 treatment. Only three metabolic pathways appeared to be deregulated after chitosan treatment when BAK1, BKK1, and CERK1 were not present or nonfunctional (Supplementary Fig. S6). Together, our data show that application of flg22 and chitosan induced the accumulation of different phytoalexin compounds following PTI activation. Moreover, simultaneous application of the two PEs induced a pattern of defense-related phytoalexin compounds, which differed from the ones produced after individual flg22 or chitosan treatments. The pattern obtained did not result in the additivity of the two individual profiles.

We further analyzed the dataset generated earlier using the Metaboanalyst 5.0 online platform (www.metaboanalyst.ca; Pang et al. 2021) with the aim of visualizing and measuring how the different PE treatments could affect the different metabolic pathways within the whole metabolome. We performed an enrichment analysis and a pathway analysis, and we obtained three distinct maps of induced metabolic pathways. The metabolic pathways with a $-\log_{10}(P)$ superior to 1.3 and pathway impact above 0.3 were considered deregulated. First, we confirmed previous observations related to PE-induced activation of phytoalexin-related pathways (Fig. 5) and the highest impact on phenylpropanoid pathways activated after the simultaneous application of both PEs (Fig. 5). Interestingly, we also found a regulation of several primary metabolism-related pathways, including amino acids, lipids as well as purine nucleic acid. Unexpectedly, simultaneous application of both PEs induced a pattern of deregulated metabolic pathways, which differed from the ones produced after individual flg22 or chitosan treatments. The pattern did not result in the additivity of both individual profiles. It also did not overlap with these individual profiles, as we observed additional metabolic pathways, which were not differentially regulated by either the single flg22 or chitosan treatment. Particularly, several primary metabolite-related metabolic pathways, including primary sugars as well as photosynthesis and lipid metabolism, were found to be regulated (Fig. 5). Together, these results strongly suggested that the simultaneous application of both flg22 and chitosan activates a unique pattern of metabolic pathways. We also analyzed the differentially regulated metabolites on WT *Arabidopsis* plantlets treated with suboptimal concentrations of PE applied individually (10 nM and 100 nM for flg22; 0.01 mg/ml and 0.1 mg/ml for chitosan) or in combination (10 nM flg22 + 0.01 mg/ml chitosan; 100 nM flg22 + 0.1 mg/ml chitosan; Supplementary Figs. S7 to S9). We found a lower total number of deregulated metabolites when compared with optimal concentration (Supplementary Fig. S7; see also Fig. 5). Also, we observed in all the combinations the same pattern: Each PE was exhibiting a specific set of deregulated metabolic pathways, while the corresponding flg22 + chitosan combination was showing a different pattern (Supplementary Figs. S8 and S9). This result is aligned with the previous findings in this study and may support the additive effect of the combination we have reported.

Finally, we analyzed the primary metabolism-derived compounds shown to be deregulated by each treatment (Fig. 6). Flg22 treatment differentially regulated 9 lipids, 8 amino acids, and 7 organic acids, whereas chitosan treatment differentially regulated 8 lipids, 9 amino acids and 4 organic acids (Fig. 6). There were no overlaps within metabolites from one treatment to another. The simultaneous application of both PEs regulated the production of 20 lipids, 19 amino acids, and 6 organic acids. Interestingly, the quantity of most lipids and organic acids decreased, while most of the deregulated amino acids were shown to accumulate (Fig. 6). These results highlight the impact of the combined elicitation on lipid and amino acid metabolites. The strong increase of amino acids after flg22 + chitosan elicitation correlates with the impact of this treatment on metabolic pathways related to primary metabolism (Fig. 5).

Discussion

Globally, the threat to food security remains partly due to plant pathogens and plant pests attacking crops (Savary et al. 2019). One possible strategy to tackle this issue is the use of PEs as part of integrated pest management practices. Yet, while PEs have been used for crop treatment for three decades under controlled conditions, many have limited efficacy in the field (Gelineo-Albersheim et al. 2018 and references therein; Sandroni et al. 2020). Several reasons can explain this lack of success, pest-management-wise. First, they are used in the field, a setting where plants are simultaneously exposed to several stresses (Atkinson and Urwin 2012; Atkinson et al. 2013). Second, several parameters can influence the outcome of the application of PE on plants, including genetic intraspecies diversity (at the cultivar level), as well as interspecies diversity of plant individuals treated with PE, the impact of age, and the impact of various agricultural practices including fertilization (Fauvergue et al. 2022).

To better understand how PEs used alone or in combination impact a plant's physiology, we chose the model plant *Arabidopsis* and focused on the well-characterized PEs flg22 and chitosan to measure both transcriptional and metabolomic responses induced by exogenous treatment with them. Notably, in previous work in *Arabidopsis* and rice, it was shown that early transcriptional changes to different PEs are mostly congruent (Asai et al. 2002; Bjornson et al. 2021; Eulgem et al. 1999; Tang et al. 2021). Notably, we used a multi-omics approach, in which PE-specific metabolomic profiles as well as posttranslational modifications were measured (using flg22 and chitin). We found that the patterns were PE-specific, thus suggesting that some PTI responses might be PE-specific (Tang et al. 2021). In our study, to better reflect the impact of long-term treatment in the field, we focused on late events (24 to 48 h) following treatment with flg22 and/or chitosan and measured metabolomic changes induced by these PEs, as secondary metabolites are often produced to fight pathogens and pests directly or indirectly (Erb and Kliebenstein 2020).

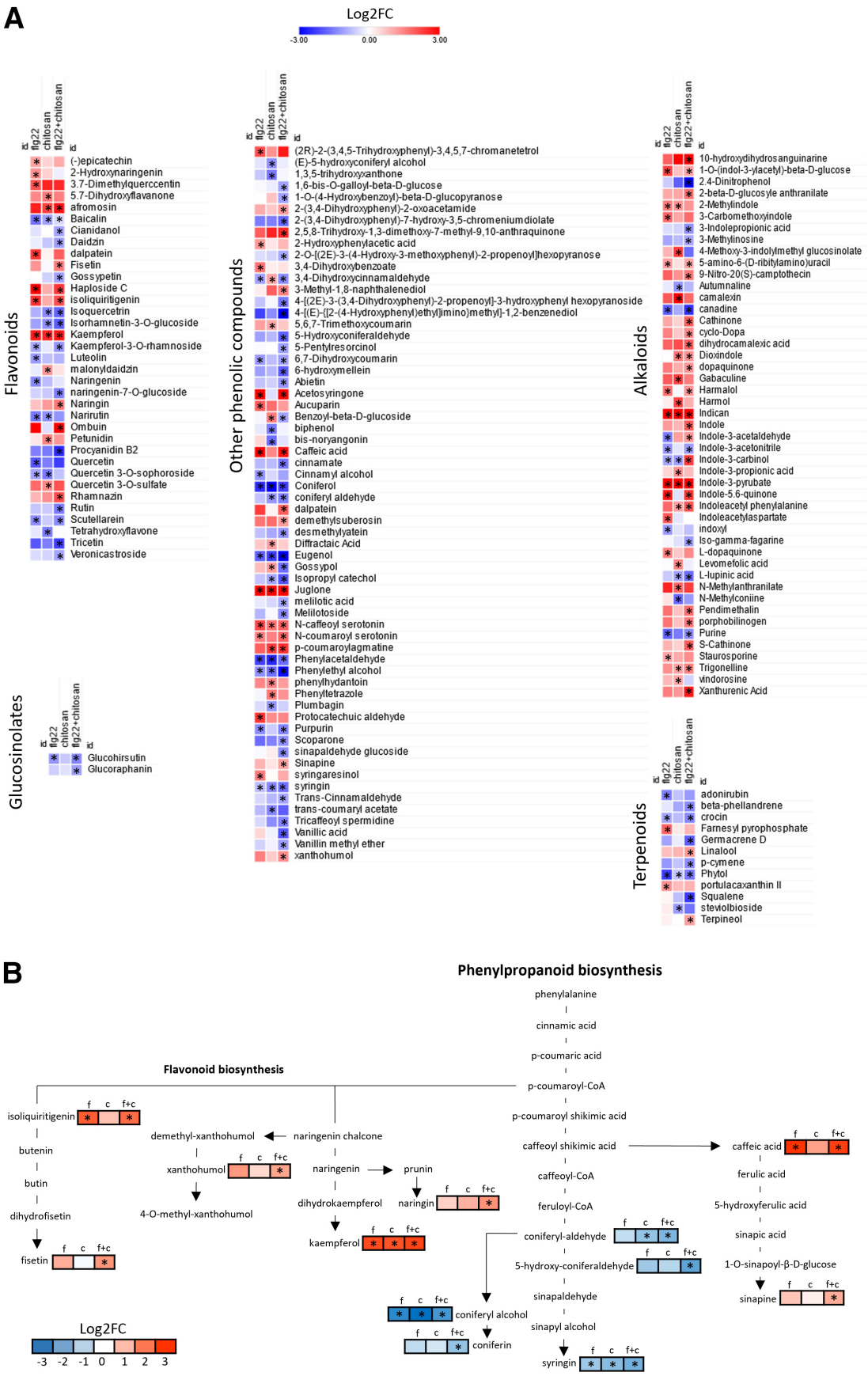

Fig. 4. Secondary metabolites significantly deregulated by plant elicitor (PE) treatments. **A,** Heat map of metabolites significantly deregulated at least in one of the conditions. Values are expressed as $\log_2$ fold change (Log2FC) of treated versus control. **B,** Effect of flg22 + chitosan treatments on phenylpropanoid biosynthesis pathway. Log2FC levels of different metabolites significantly deregulated at least in flg22 + chitosan treatments. An asterisk (*) indicates a significant difference compared with the control (fold changes > 2 or < 0.5, *P* value < 0.05). Increase of metabolite quantity following elicitation is shown in red, decrease in blue, and no change in white. f, flg22; c, chitosan; f + c, flg22 + chitosan.

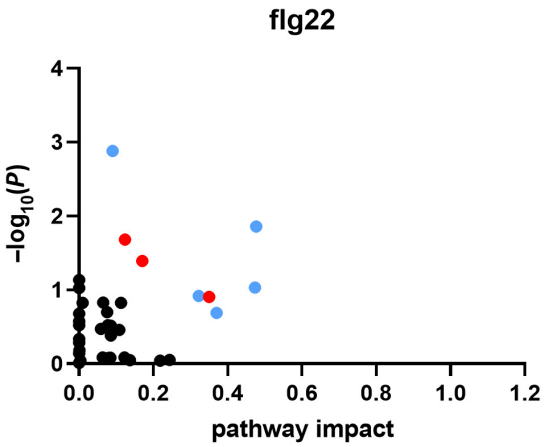

Pathway Name	−log(*P*)	Impact
Phenylalanine, tyrosine and tryptophan biosynthesis	**2.8808**	0.09009
Tryptophan metabolism	**1.8577**	0.47684
Glucosinolate biosynthesis	**1.6823**	0.12399
Flavonoid biosynthesis	**1.391**	0.17065
Glutathione metabolism	1.0306	**0.47348**
Cyanoamino acid metabolism	0.91936	**0.32203**
Flavone and flavonol biosynthesis	0.9057	**0.35**
Alanine, aspartate and glutamate metabolism	0.68804	**0.37051**

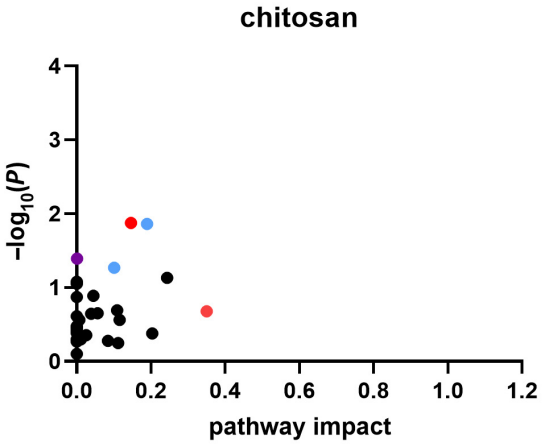

Pathway Name	−log(*P*)	Impact
Phenylpropanoid biosynthesis	**1.8747**	0.14664
Tryptophan metabolism	**1.8611**	0.18981
Pyrimidine metabolism	**1.391**	0.00107
Arginine biosynthesis	**1.2669**	0.10097
Flavone and flavonol biosynthesis	0.6772	**0.35**

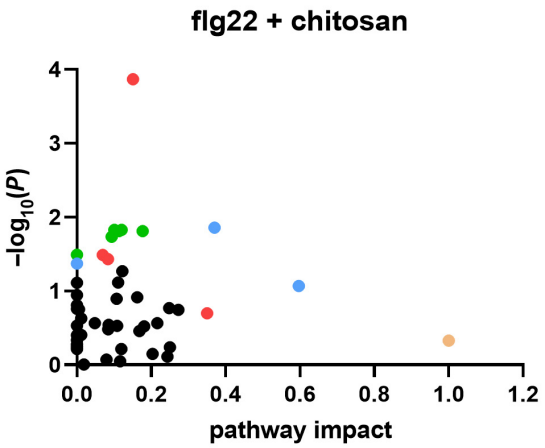

Pathway Name	−log(*P*)	Impact
Phenylpropanoid biosynthesis	**3.8699**	0.15089
Alanine, aspartate and glutamate metabolism	**1.8576**	0.37051
Glycolysis/Gluconeogenesis	**1.8272**	0.12036
Carbon fixation in photosynthetic organisms	**1.8272**	0.10075
Pyruvate metabolism	**1.8122**	0.17693
Citrate cycle (TCA cycle)	**1.8122**	0.11277
Glyoxylate and dicarboxylate metabolism	**1.7335**	0.09355
Valine, leucine and isoleucine degradation	**1.4908**	0.0
Flavonoid biosynthesis	**1.4872**	0.06983
Glucosinolate biosynthesis	**1.4318**	0.08394
Phenylalanine, tyrosine and tryptophan biosynthesis	**1.3706**	0.0
Tryptophan metabolism	1.0688	**0.59721**
Flavone and flavonol biosynthesis	0.69852	**0.35**
Linoleic acid metabolism	0.32923	**1.0**

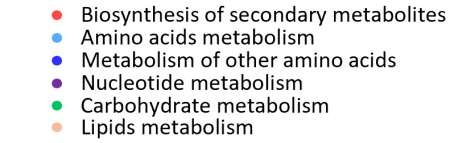

Fig. 5. The metabolic pathways most impacted by plant elicitor (PE) treatments. Metabolic pathway analytical plots were created using MetaboAnalyst 5.0. The *x* axis represents the pathway impact value computed from the pathway topological analysis, and the *y* axis is the $\log_{10}$ of the *P* value obtained from pathway enrichment analysis. The pathways that were the most significantly changed are characterized by both a high log(*P*) value ($-\log_{10}(P) > 1.3$) and high-impact value (top right region, pathway impact > 0.3). The colors of the dots indicate the category of the most-impacted pathway according to KEGG orthology. The most significantly changed pathways are listed next to each graph.

Some studies have investigated and compared the metabolome of PE-treated plants. They found that different PEs, once applied to plants, led to metabolite deregulation. This was demonstrated in potato when PAMP- and non-PAMP-PEs were compared (Martin et al. 2020). It was also the case when PAMP-PEs were tested on rice (Tang et al. 2021) or in tomato (Zeiss et al. 2021).

In the current study, we found that each PE treatment induced a unique metabolomic profile (Figs. 4 and 7). Moreover, double elicitation with flg22 + chitosan yielded a third, enriched metabolomic profile (Figs. 4 and 7). While families of upregulated compounds were preserved following flg22 or chitosan treatment, some families/subfamilies of compounds seemed activated by flg22 but not by chitosan. For instance, flg22 treatment specifically yielded lignan lactone secondary metabolites, while chitosan did not. Among other groups of secondary metabolites, flg22 treatment yielded more subfamilies of metabolites. Conversely, chitosan treatment yielded more subfamilies of organoheterocyclic compounds. It is noteworthy that such contrasting effects of PE treatments upon single or concomitant application have already been monitored by focusing on very early events following PTI activation (Aslam et al. 2009). We also observed a significant deregulation of primary metabolites, including amino acids, lipids, and organic acids (Fig. 6). Amino acids (Liu et al. 2010), lipids (Mandal et al. 2012), and organic acids (Rojas et al. 2012) are known to be deregulated upon PE application (for a review, see Rojas et al. 2014). Further, double elicitation accentuated this deregulation (Fig. 6). This increase in deregulation of primary metabolites may accompany the accumulation of

Fig. 6. Lipids, amino acids, and organic acids significantly deregulated by plant elicitor (PE) treatments. Heat map of metabolites significantly deregulated in at least one of the conditions. An asterisk (*) indicates a significant difference with the control (fold change > 2 or < 0.5, P value < 0.05). Values are expressed as $\log_2$ fold change (Log2FC) of treated versus control. Upregulation after elicitation is shown in red, downregulation in blue, and no change in white.

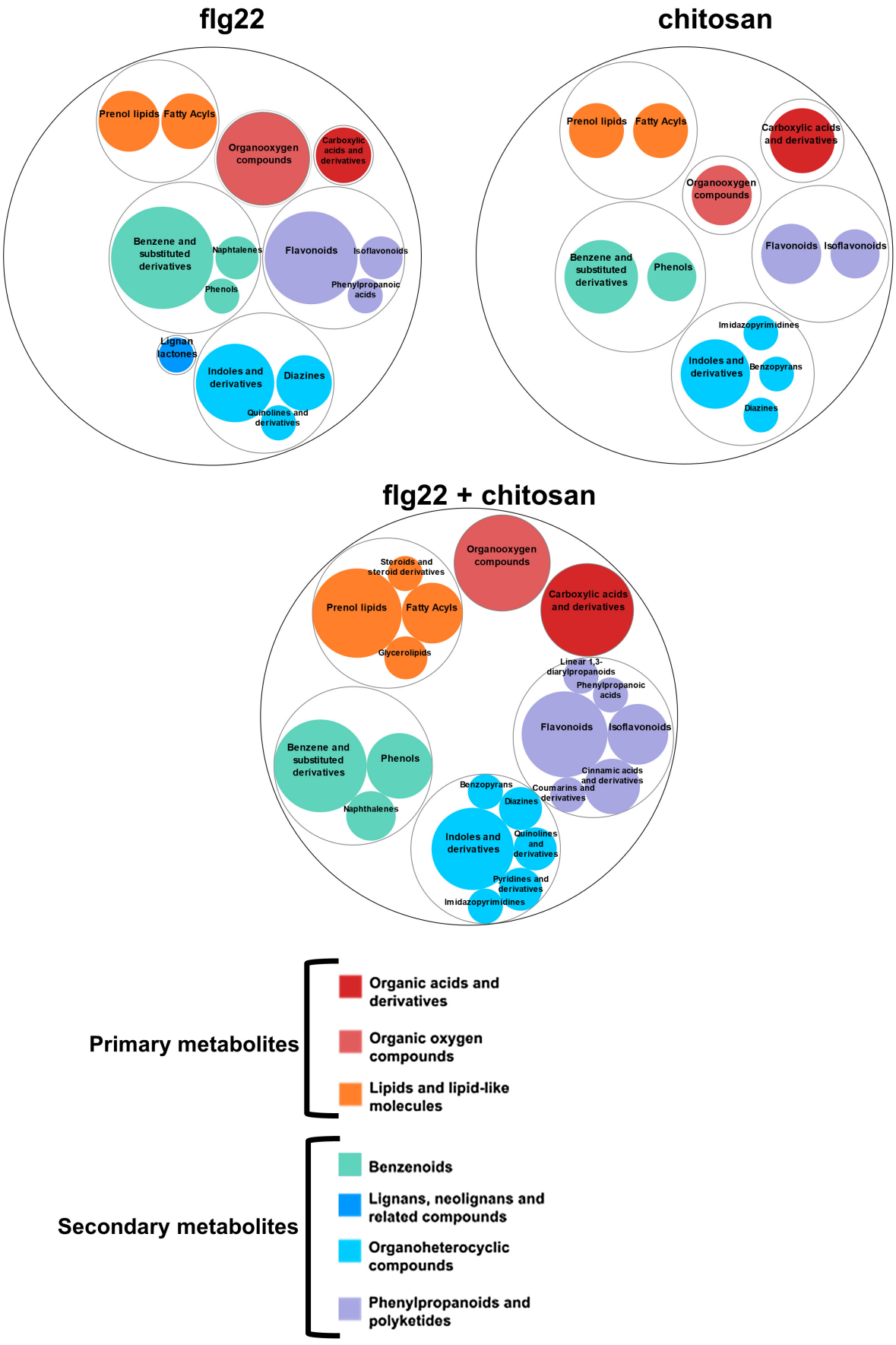

Fig. 7. Overview of metabolic deregulation induced by plant elicitor (PE) treatments. Circular treemap of classification of metabolites significantly deregulated in at least one of the conditions. Metabolites are classified by their structures according to ClassyFire (Djoumbou Feunang et al. 2016). The size of the circle indicates the number of metabolites belonging to the same class. Primary metabolites are shown in warm colors; secondary metabolites are shown in cool colors.

secondary metabolites (Fig. 5). A proper experimental design is needed to appropriately confirm this hypothesis. Additionally, the finding that flg22-induced plants yielded a higher SA content compared with those treated with flg22 + chitosan was also intriguing. It is known that chitosan can increase the levels of both SA and jasmonic acid (JA) (Jia et al. 2018). This unusual effect of chitosan may explain the observed suppression of flg22-induced SA by chitosan, given the known antagonism between SA and JA. It will thus be important in future studies to test how different PE treatments impact infection by different pathogens that might show contrasting sensitivities to diverse plant compounds. Interestingly, when flg22 and chitosan were applied concomitantly, we did not immediately observe an important enrichment of metabolites: While no additional group of primary and secondary metabolites was reported, a noticeable increase in the number of subfamilies within several groups of metabolites was visible (Fig. 7). Yet, despite the differential metabolic response observed upon combined elicitation in plantlets, no statistically significant additive effect on the induced resistance to the phytopathogenic bacterium *Pto* DC3000 could be measured (Fig. 2). In this context, it is interesting to note that a simultaneous application of PEs was previously shown to even decrease IR efficacy (Bartels et al. 2013; Souza et al. 2017). Both our and these previous results are particularly puzzling, considering the reported cross-activation of *AtCERK1* (the co-receptor for chitin/chitosan) by *AtBAK1* (the co-receptor for flg22) (Gong et al. 2019).

In conclusion, our work provides grounds for future research into understanding how early and late responses induced by different PEs intersect (positively, and potentially even negatively), and how this information can ultimately be used under field conditions to improve crop treatment against pests and pathogens. This is particularly important, as some natural extracts used for crop treatment might contain more than one active PE. For instance, an *Ulva lactuca* extract exhibiting defense-eliciting properties contains ulvan polysaccharides (de Borba et al. 2021; Cluzet et al. 2004; Martin et al. 2020) but was recently shown to also contain arabinogalactan-like proteins able to mount a PE-dependent IR (Přerovská et al. 2022).

Materials and Methods

Culture conditions

Lines of *Arabidopsis thaliana* L. (Heynh.) used in this study were as follows: WT 'Columbia', *cerk1* (Gabi mutant 096F09) (Miya et al. 2007), *fls2* (Zipfel et al. 2004), *fls2 efr cerk1* (*fec*) (Xin et al. 2016), *bak1-5 bkk1* (Schwessinger et al. 2011), and *bak1-5 bkk1 cerk1* (Xin et al. 2016). Unless indicated otherwise, seedlings were grown on vertical Petri plates containing nutrient-solidified agar in a phytotron (16 h of light with photosynthetic photon flux density ranging from 260 to 330 µmol photons/m^2/s^1 and 8 h of dark at 21°C and 19°C, respectively) for 10 days, as described in Nguema-Ona et al. (2007). Briefly, WT and mutant seeds were surface-sterilized for 5 min in 70% (vol/vol) ethanol and 2 min in 3% (vol/vol) bleach, then washed six times in sterile water, and finally stratified for 48 h at 4°C. Seeds were sown in solid 0.5× MS medium, pH 5.8, containing 0.7% agar (A1296 Sigma-Aldrich) and 1.2% sucrose (35508 Alfa Aesar). For some experiments, 4- to 5-week-old *Arabidopsis thaliana* Col-0 plants were grown at 22°C, 60% humidity, 10-h/14-h light/dark, and a light intensity of 120 µmol/m^2.

Elicitors

Flg22 peptide (QRLSTGSRINSAKDDAAGLQIA) was synthetized using the PRIMACEN platform, Peptide Synthesis Platform (Université de Rouen Normandie) or ordered from SciLight Biotechnology LLC. Chitosan was supplied by Sigma-Aldrich (448869).

Seedling elicitation

Arabidopsis seedlings were treated with either flg22 (from 10 nM to 1 µM), chitosan (from 0.01 to 100 mg/liter), a combination of both, or sterile water as negative control following a procedure adapted from (Zahid et al. 2017). Briefly, plantlets were immersed in water supplemented with the different elicitors. After 30 min, the media was removed, and the seedlings were replaced in the phytotron. Plantlets were harvested at the appropriate hours posttreatment (hpt).

ROS detection

After 30 min of elicitation, ROS were detected by incubating the seedling in NBT (Choi et al. 2006) solution at 0.05% (wt/vol) in phosphate buffer (K_2HPO_4 100 mM, pH 7.5) for 90 min. Seedlings were washed three times in the phosphate buffer and fixed in ethanol/acetic acid (3:1 vol/vol) solution for 2 h. The samples were put successively in 70%, 50%, and 30% ethanol solutions for 90 min, allowing a progressive rehydration of the tissues. Seedlings were incubated in water overnight before being treated with an NaOH 10% solution for 1 h at 37°C. ROS accumulation stained in dark blue was observed with a binocular microscope (Leica M125). Images were acquired with a DFC295 camera (Leica). ROS quantification was assessed using ImageJ software (Abramoff et al. 2004).

For ROS detection using the luminol/peroxidase assay, we followed the protocol established by Kadota et al. (2015) with minor modifications. In brief, leaf disks of approximately 4 mm in diameter were excised from 4- to 5-week-old *Arabidopsis thaliana* (Col-0 WT) plants grown at 22°C, 60% humidity, 10-h/14-h light/dark, and a light intensity of 120 µmol/m^2. A minimum of 12 leaf disks per treatment were collected. Following excision, the leaf disks were placed in a 96-well plate filled with water and subjected to an overnight incubation period to facilitate the acclimatization of the disks to the new environment and to allow wound-induced responses to subside. Following the incubation period, the water in each well was replaced with a solution composed of 1 µM L-012 (a highly sensitive chemiluminescent probe that reacts with horseradish peroxidase [HRP]), 20 µg/ml/liter HRP (a catalyst that accelerates the oxidation of L-012), and 100 nM flg22 (QRLSTGSRINSAKDDAAGLQIA) peptide obtained from SciLight Biotechnology LLC. After elicitation, the luminescence emitted by the solution was quantified over a duration of approximately 40 min using a Tecan Spark Multi-Plate Reader. The light emitted from the solution was directly proportional to the ROS concentration, allowing for a quantitative assessment of ROS production.

Callose staining

Callose detection was performed as described in Zahid et al. (2017) using decolorized aniline blue staining. Following the 30 min of elicitation, seedlings were placed for 48 h in the phytotron before being fixed and discolored in acetic acid/ethanol (1:3 vol/vol) for 2 h. Samples were rehydrated by successive ethanol treatments at 75%, 50%, 25% (vol/vol) for 2 h and finally with water overnight before being incubated with 10% (wt/vol) NaOH at 37°C for 1 h and then overnight in 0.01% (wt/vol) aniline blue solution (150 mM K_2HPO_4 at pH 10). Seedlings were mounted on slides, and callose deposition was observed with an epifluorescence microscope (Leica DMI 6000 B, camera DFC 450 C).

Induced resistance assay to *Pto* DC3000

Arabidopsis seeds were surface-sterilized, stratified for 3 to 5 days, and planted on soil. Plants were grown for 4 to 5 weeks at

22°C, 60% humidity, 10-h/14-h light/dark before induced resistance assays were performed. Bacterial infection assays were performed as described previously (Zipfel et al. 2004). *Pto* DC3000 was grown in overnight culture in King's B medium (20 g/liter proteose, 1.5 g/liter dipotassium hydrogen phosphate, and 15 g/liter glycerol) supplemented with 10 μg/ml rifampicin and incubated at 28°C with shaking (220 rpm). For induced resistance assays, 4- to 5-week-old *Arabidopsis* plants were used. Three leaves from each plant were pretreated (24 h before infiltration with *Pto* DC3000) with the following treatment combinations: distilled water (mock); flg22 from 10 nM to 1 μM (Scilight-Peptide); and chitosan from 0.01 to 1 mg/liter (no. 448869, Sigma-Aldrich). Bacteria grown overnight were first refreshed through a 1- to 2-h subculture in 1:10 volume of overnight culture on fresh LB medium. Refreshed cells were then harvested by centrifugation, and pellets were resuspended in 10 mM $MgCl_2$. Selected leaves were reinfiltrated with *Pto* DC3000 at $OD_{600} = 0.0002$ or $\sim 1 \times 10^5$ colony-forming units (CFUs)/ml. After 48 h of inoculation, two leaf disks were collected from each infiltrated leaf and ground in 10 mM $MgCl_2$, and serial dilutions from 1×10^{-1} to 1×10^{-5} were plated on LB medium supplemented with 10 μg/ml rifampicin and incubated at 28°C for 2 days. The bacterial growth was measured by counting the CFUs. Analysis of variance (ANOVA) was performed using the ANOVA functions in GraphPad Prism version 9.0 (http://www.graphpad.com), and multiple pairwise comparisons were performed using Tukey's honest significant difference method. Sample numbers for induced resistance assays were $n = 12$ plants for all genotype–treatment combinations. Statistical analysis was performed in GraphPad Prism 9.0. (GraphPad software, http://www.graphpad.com). Differences between groups were significant at a P value of < 0.05.

Marker gene expression by reverse transcription-quantitative PCR (RT-qPCR)

For each harvest time, three biological replicates (three independent cultures) were carried out, and subsequently, independent RNA extractions were done for each replicate. The consumables and solutions used to work with RNAs were certified RNase-free, and the experiments were carried out in an RNase-free environment.

Total RNA was purified from four plantlets (i.e., 50 to 60 mg of fresh material) with the NucleoSpin RNA Plus kit (Macherey-Nagel) according to the supplier's protocol. At harvest time, the seedlings were put in 350 μl of LBP buffer in a 2-ml lysing matrix tube E (MP Biomedicals), and the samples were stored at –80°C until RNA extraction. Lysis of the cells was carried out by four runs of 30 s at 6.5 m/s in a FastPrep-24 Homogenizer instrument (MP Biomedicals). Total RNA was finally eluted in 60 μl of RNase-free water and stored at –80°C until further use. For each sample, an aliquot was removed to evaluate the RNA concentration with a Nanodrop 2000c spectrophotometer (Thermo Scientific). Ten milligrams of RNA was digested with 2U of TURBO DNaseTM (Invitrogen) in a final volume of 50 ml at 37°C for 30 min, followed by 25°C for 5 min after adding 5 μl of DNase inactivation reagent (provided by the supplier). cDNA was then synthesized from 2 μg of total RNA with the High-capacity cDNA reverse transcription kit from Applied Biosystems with total RNA samples in a final reaction volume of 20 ml, following the manufacturer's instructions. The cDNAs were then stored at –20°C until use. The qPCR was carried out with the QuantStudio 12K Flex Real-Time PCR System (Applied Biosystems), and the pipetting steps were done with the Bravo Automated Liquid Handling Platform (Agilent Technologies). The reaction mix was prepared in a 384-well reaction plate: 1.2 ml of a 1/10 dilution of cDNA was mixed with 0.3 μM of each primer pair in a 5-μl total reaction using the Fast SYBR Green PCR Master Mix (Applied Biosystems). PCR amplification was carried out using the following amplification protocol: 20 s at 95°C, then 40 cycles of 3 s at 95°C, 20 s at 60°C, followed by the melt-curve analysis: 15 s at 95°C, 1 min at 60°C, and 15 s at 95°C. Primer pairs specific to each selected gene were defined using either Primer3plus or the literature (Supplementary Table S2). The oligonucleotides (desalted quality) were synthesized by Eurogentec (Kaneka Eurogentec S.A). To validate the primer pairs, a dilution set of cDNA was prepared as follows: first, a 1/10 dilution of the cDNA stock was prepared, and four consecutive 1/3 dilutions were made from it, and the five cDNA dilutions were used in the RT-qPCR experiment to test each pair of primers and determine the optimal cDNA dilution to use. Data were analyzed using the ΔΔCT method with *ROC3* (AT2G16600) as an endogenous reference (Kanno et al. 2016).

Determination of phytohormones

SA was purchased from Sigma-Aldrich and Olchemln. Stable isotope-labeled internal standard, d4-SA, was ordered from the National Research Council of Canada (Ottawa, Canada) and OlchemIn. Sample preparation and phytohormone content determination were performed as described in Lakkis et al. (2019) and Martin et al. (2020). Briefly, phytohormones were extracted from 10 mg of liquid nitrogen ground plantlet material, collected at 24 and 48 hpt, in 1 ml of cold solution of methanol/water/formic acid (70:29:1 vol/vol/vol). Isotope-labeled internal standard was pre-diluted in the formic acid organic solvent present in the cold methanol/water/formic acid solution. The homogenates were stirred at room temperature and centrifuged at 12,600 rpm to collect the supernatant. After evaporation (SPE Dry 96, Biotage), the extract was resuspended in 2% formic acid solution and purified using a, SPE ABN (solid phase extraction, acidic, basic and neutral analytes) express plate of 30 mg/ml (Biotage). The phytohormones were eluted with methanol, and the samples were evaporated and resuspended in 200 ml of 0.1% formic acid solution before being injected into the system. The separation and detection were achieved using a Nexera X2 UHPLC system coupled to a QTrap 6,500 C mass spectrometer equipped with an IonDrive turbo V electrospray source. Phytohormone separation was carried out by injecting a 2-ml sample into a Kinetex Evo C18 core–shell column (100 × 2.1 mm, 2.6 μm, Phenomenex) at a flow rate of 0.7 ml/min, and the column temperature was maintained at 40°C. The mobile phases were composed of solvent A Milli-Q water containing 0.1% formic acid (LCMS grade, Fluka Analytics), and solvent B acetonitrile LCMS grade containing 0.1% formic acid. The gradient elution started with 1% of B, 0.0 to 5.0 min 60% of B, 5.0 to 5.5 min 100% of B, 5.5 to 7.0 min 100% of B, 7.0 to 7.5 min 1% of B, and 7.5 to 9.5 min 1% of B. The analysis was performed in a scheduled MRM mode in positive and negative modes simultaneously with a polarity switching of 5 ms: ion spray voltage was 5,500 V in the positive mode and 4,500 V in the negative mode; source temperature was 600°C; curtain gas at 35 psi; nebulizer gas at 50 psi; heater gas at 60 psi; collision gas at medium; entrance potential of ±10 V; MRM detection window of 30 s; target scan time of 0.075 s. An external calibration curve was established. A quality-control (QC) sample containing all external and internal standards was injected every 10 samples to access the system stability. The calculated concentration was corrected by the internal standard recovery rate.

Untargeted metabolic profiling using UPLC-MS/MS

Plant material was harvested as follows: each assay was repeated three times, consisting of two individual repetitions (independent biological repetitions) for a total of six repetitions. Fifty milligrams of ground frozen seedling tissues harvested at 24 hpt

were weighed and extracted with 1 ml of 70% MeOH (Optima LCMS grade, Fisher), 29% water (Milli-Q, 18.2 MΩ·cm, Millipore), and 1% formic acid (LCMS grade, Fluka Analytics). After extraction, samples were centrifuged, and the supernatant was collected for UPLC-MS/MS analysis. For the UPLC-MS/MS analysis, the separation and the detection were accomplished using an Acquity UPLC system (Waters) coupled to a Xevo G2-S QTof mass spectrometer (Waters) equipped with an LockSpray electrospray ionization source. Sample separation was carried out by injecting 10 µl into an HSS T3 C18, 2.1 × 100 mm, 1.8-µm column (Waters) at a flow rate of 0.5 ml/min, and the column oven was maintained at 40°C. The mobile phases were composed of solvent A Milli-Q water containing 0.1% formic acid and solvent B acetonitrile containing 0.1% formic acid. The separation was achieved by the following gradient: 0 to 1 min at 98% A, 1 to 7 min from 98% to 0% A, maintained at 0% A to 9 min, 9 to 10 min from 0% to 98% A, maintained at 98% until 12 min for column regeneration. The MS analysis was carried out respectively in positive and negative ionization modes with the following parameters: source voltage of 0.5 kV (pos) and 2.5 kV (neg); cone voltage of 40 V; source temperature of 130°C; desolvation gas temperature of 550°C; desolvation gas flow of 900 liters/h. Mass spectra were acquired in MSE mode from 50 to 1200 *m*/*z* at 0.1 s/scan. The ramp collision energy was set at 25 to 40 V. Samples were injected in randomized order. A QC sample was prepared from an equal mix of all collected samples. The QC sample was injected every eight samples to assess system stability. After the acquisition, metabolomic data were processed using Progenesis QI software (version 3.0, Waters). Identification was carried out using the PlantCyc database (version 15.0.1) (https://www.plantcyc.org) with a mass tolerance of 10 ppm. For identified metabolites, experimental MS2 spectra were compared with the MS-DIAL reference MS/MS database (version 14) (Tsugawa et al. 2015) when possible, otherwise they were compared with the theoretical fragmentation spectrum. The fragment mass tolerance was set at 10 ppm. Only identified metabolites were used for further analysis.

Univariate analysis (Student's *t*-test) was performed for statistical testing (Wu et al. 2021). The metabolites with a P value < 0.05 and fold-change > 2 were kept and considered to be supposedly statistically significant. Volcano plots were generated using VolcaNoseR (Goedhart and Luijsterburg 2020). A Venn diagram was generated with jvenn (Bardou et al. 2014), and pathway analysis was done using MetaboAnalyst 5.0 (Pang et al. 2021). For each pathway, the P value of metabolite set enrichment analysis and pathway impact of topology analysis were calculated using the KEGG database (Kanehisa et al. 2017). All the significant metabolites deregulated in each treatment were categorized by classes, and heat maps were created using Morpheus software (https://software.broadinstitute.org/morpheus). The circular treemaps were generated using RAWGraphs 2.0 (Mauri et al. 2017).

Acknowledgments

E. Nguema-Ona is grateful to Azeddine Driouich and Maité Vicré (Université de Rouen Normandie, France) and Thibaut Malausa (INRAe, France) for the critical reading of the manuscript. Initial work on the PE-specific patterns during late events following PTI activation was performed with Florence Val (Institut Agro–Université de Rennes, France, 2017 to 2020). Damien Souquet and Bastien Billiot (CMI- Roullier) are acknowledged for their help in building an algorithm for data analyses. Thomas Badou (Université de Rouen) is also acknowledged for his help with some additional experiments.

Literature Cited

Abramoff, M. D., Magalhães, P. J., and Ram, S. J. 2004. Image processing with ImageJ. Biophoton. Int. 11:36-42.

Ahuja, I., Kissen, R., and Bones, A. M. 2012. Phytoalexins in defense against pathogens. Trends Plant Sci. 17:73-90.

Asai, T., Tena, G., Plotnikova, J., Willmann, M. R., Chiu, W.-L., Gomez-Gomez, L., Boller, T., Ausubel, F. M., and Sheen, J. 2002. MAP kinase signalling cascade in *Arabidopsis* innate immunity. Nature 415:977-983.

Aslam, S. N., Erbs, G., Morrissey, K. L., Newman, M.-A., Chinchilla, D., Boller, T., Molinaro, A., Jackson, R. W., and Cooper, R. M. 2009. Microbe-associated molecular pattern (MAMP) signatures, synergy, size and charge: Influences on perception or mobility and host defence responses. Mol. Plant Pathol. 10:375-387.

Atkinson, N. J., Lilley, C. J., and Urwin, P. E. 2013. Identification of genes involved in the response of Arabidopsis to simultaneous biotic and abiotic stresses. Plant Physiol. 162:2028-2041.

Atkinson, N. J., and Urwin, P. E. 2012. The interaction of plant biotic and abiotic stresses: From genes to the field. J. Exp. Bot. 63:3523-3543.

Bardou, P., Mariette, J., Escudié, F., Djemiel, C., and Klopp, C. 2014. jvenn: An interactive Venn diagram viewer. BMC Bioinfo. 15:293.

Bartels, S., Lori, M., Mbengue, M., van Verk, M., Klauser, D., Hander, T., Böni, R., Robatzek, S., and Boller, T. 2013. The family of Peps and their precursors in *Arabidopsis*: Differential expression and localization but similar induction of pattern-triggered immune responses. J. Exp. Bot. 64:5309-5321.

Bjornson, M., Pimprikar, P., Nürnberger, T., and Zipfel, C. 2021. The transcriptional landscape of *Arabidopsis thaliana* pattern-triggered immunity. Nat. Plants 7:579-586.

Boller, T., and Felix, G. 2009. A renaissance of elicitors: Perception of microbe-associated molecular patterns and danger signals by pattern-recognition receptors. Annu. Rev. Plant Biol. 60:379-406.

Boutrot, F., and Zipfel, C. 2017. Function, discovery, and exploitation of plant pattern recognition receptors for broad-spectrum disease resistance. Annu. Rev. Phytopathol. 55:257-286.

Cao, Y., Liang, Y., Tanaka, K., Nguyen, C. T., Jedrzejczak, R. P., Joachimiak, A., and Stacey, G. 2014. The kinase LYK5 is a major chitin receptor in *Arabidopsis* and forms a chitin-induced complex with related kinase CERK1. eLife 3:e03766.

Chae, L., Kim, T., Nilo-Poyanco, R., and Rhee, S. Y. 2014. Genomic signatures of specialized metabolism in plants. Science 344:510-513.

Chinchilla, D., Zipfel, C., Robatzek, S., Kemmerling, B., Nürnberger, T., Jones, J. D. G., Felix, G., and Boller, T. 2007. A flagellin-induced complex of the receptor FLS2 and BAK1 initiates plant defence. Nature 448:497-500.

Chisholm, S. T., Coaker, G., Day, B., and Staskawicz, B. J. 2006. Host-microbe interactions: Shaping the evolution of the plant immune response. Cell 124:803-814.

Choi, H. S., Kim, J. W., Cha, Y.-N., and Kim, C. 2006. A quantitative nitroblue tetrazolium assay for determining intracellular superoxide anion production in phagocytic cells. J. Immunoassay Immunochem. 27:31-44.

Cluzet, S., Torregrosa, C., Jacquet, C., Lafitte, C., Fournier, J., Mercier, L., Salamagne, S., Briand, X., Esquerré-Tugayé, M.-T., and Dumas, B. 2004. Gene expression profiling and protection of *Medicago truncatula* against a fungal infection in response to an elicitor from green algae *Ulva* spp. Plant Cell Environ. 27:917-928.

de Borba, M. C., Velho, A. C., Maia-Grondard, A., Baltenweck, R., Magnin-Robert, M., Randoux, B., Holvoet, M., Hilbert, J.-L., Flahaut, C., Reignault, P., Hugueney, P., Stadnik, M. J., and Siah, A. 2021. The algal polysaccharide ulvan induces resistance in wheat against *Zymoseptoria tritici* without major alteration of leaf metabolome. Front. Plant Sci. 12:703712.

DeFalco, T. A., and Zipfel, C. 2021. Molecular mechanisms of early plant pattern-triggered immune signaling. Mol. Cell 81:3449-3467.

Djoumbou Feunang, Y., Eisner, R., Knox, C., Chepelev, L., Hastings, J., Owen, G., Fahy, E., Steinbeck, C., Subramanian, S., Bolton, E., Greiner, R., and Wishart, D. S. 2016. ClassyFire: Automated chemical classification with a comprehensive, computable taxonomy. J. Cheminform. 8:61.

Erb, M., and Kliebenstein, D. J. 2020. Plant secondary metabolites as defenses, regulators, and primary metabolites: The blurred functional trichotomy. Plant Physiol. 184:39-52.

Eulgem, T., Rushton, P. J., Schmelzer, E., Hahlbrock, K., and Somssich, I. E. 1999. Early nuclear events in plant defence signalling: Rapid gene activation by WRKY transcription factors. EMBO J. 18:4689-4699.

Fauvergue, X., Rusch, A., Barret, M., Bardin, M., Jacquin-Joly, E., Malausa, T., and Lannou, C. 2022. Extended Biocontrol. Springer, Dordrecht, Netherlands.

Felix, G., Duran, J. D., Volko, S., and Boller, T. 1999. Plants have a sensitive perception system for the most conserved domain of bacterial flagellin. Plant J. 18:265-276.

Felix, G., Regenass, M., and Boller, T. 1993. Specific perception of subnanomolar concentrations of chitin fragments by tomato cells: Induction

of extracellular alkalinization, changes in protein phosphorylation, and establishment of a refractory state. Plant J. 4:307-316.
Gelineo-Albersheim, I., Darvill, A., and Howard, K. 2018. Peter Albersheim: 30 March 1934–23 July 2017. Glycobiology 28:714-718.
Goedhart, J., and Luijsterburg, M. S. 2020. VolcaNoseR is a web app for creating, exploring, labeling and sharing volcano plots. Sci. Rep. 10:20560.
Gómez-Gómez, L., and Boller, T. 2000. FLS2: An LRR receptor–like kinase involved in the perception of the bacterial elicitor flagellin in *Arabidopsis*. Mol. Cell 5:1003-1011.
Gong, B.-Q., Guo, J., Zhang, N., Yao, X., Wang, H.-B., and Li, J.-F. 2019. Cross-microbial protection via priming a conserved immune co-receptor through juxtamembrane phosphorylation in plants. Cell Host Microbe 26:810-822.e7.
Gubaeva, E., Gubaev, A., Melcher, R. L. J., Cord-Landwehr, S., Singh, R., El Gueddari, N. E., and Moerschbacher, B. M. 2018. 'Slipped sandwich' model for chitin and chitosan perception in *Arabidopsis*. Mol. Plant-Microbe Interact. 31:1145-1153.
Gust, A. A., Pruitt, R., and Nürnberger, T. 2017. Sensing danger: Key to activating plant immunity. Trends Plant Sci. 22:779-791.
Hahn, M. G., Darvill, A. G., and Albersheim, P. 1981. Host-pathogen Interactions : XIX. The endogenous elicitor, a fragment of a plant cell wall polysaccharide that elicits phytoalexin accumulation in soybeans. Plant Physiol. 68:1161-1169.
Heese, A., Hann, D. R., Gimenez-Ibanez, S., Jones, A. M. E., He, K., Li, J., Schroeder, J. I., Peck, S. C., and Rathjen, J. P. 2007. The receptor-like kinase SERK3/BAK1 is a central regulator of innate immunity in plants. Proc. Natl. Acad. Sci. U.S.A. 104:12217-12222.
Hou, S., Liu, Z., Shen, H., and Wu, D. 2019. Damage-associated molecular pattern-triggered immunity in plants. Front. Plant Sci. 10:646.
Jia, X., Zeng, H., Wang, W., Zhang, F., and Yin, H. 2018. Chitosan oligosaccharide induces resistance to *Pseudomonas syringae* pv. *tomato* DC3000 in *Arabidopsis thaliana* by activating both salicylic acid– and jasmonic acid–mediated pathways. Mol. Plant-Microbe Interact. 31:1271-1279.
Jones, J. D. G., and Dangl, J. L. 2006. The plant immune system. Nature 444:323-329.
Kadota, Y., Shirasu, K., and Zipfel, C. 2015. Regulation of the NADPH oxidase RBOHD during plant immunity. Plant Cell Physiol. 56:1472-1480.
Kanehisa, M., Furumichi, M., Tanabe, M., Sato, Y., and Morishima, K. 2017. KEGG: New perspectives on genomes, pathways, diseases and drugs. Nucleic Acids Res. 45:D353-D361.
Kanno, S., Arrighi, J.-F., Chiarenza, S., Bayle, V., Berthomé, R., Péret, B., Javot, H., Delannoy, E., Marin, E., Nakanishi, T. M., Thibaud, M.-C., and Nussaume, L. 2016. A novel role for the root cap in phosphate uptake and homeostasis. eLife 5:e14577.
Klarzynski, O., Plesse, B., Joubert, J.-M., Yvin, J.-C., Kopp, M., Kloareg, B., and Fritig, B. 2000. Linear β-1,3 glucans are elicitors of defense responses in tobacco. Plant Physiol. 124:1027-1038.
Lakkis, S., Trotel-Aziz, P., Rabenoelina, F., Schwarzenberg, A., Nguema-Ona, E., Clément, C., and Aziz, A. 2019. Strengthening grapevine resistance by *Pseudomonas fluorescens* PTA-CT2 relies on distinct defense pathways in susceptible and partially resistant genotypes to downy mildew and gray mold diseases. Front. Plant Sci. 10:1112.
Langner, T., Kamoun, S., and Belhaj, K. 2018. CRISPR crops: Plant genome editing toward disease resistance. Annu. Rev. Phytopathol. 56:479-512.
Liu, G., Ji, Y., Bhuiyan, N. H., Pilot, G., Selvaraj, G., Zou, J., and Wei, Y. 2010. Amino acid homeostasis modulates salicylic acid-associated redox status and defense responses in *Arabidopsis*. Plant Cell 22: 3845-3863.
Liu, T., Liu, Z., Song, C., Hu, Y., Han, Z., She, J., Fan, F., Wang, J., Jin, C., Chang, J., Zhou, J.-M., and Chai, J. 2012. Chitin-induced dimerization activates a plant immune receptor. Science 336:1160-1164.
Luna, E., Pastor, V., Robert, J., Flors, V., Mauch-Mani, B., and Ton, J. 2011. Callose deposition: A multifaceted plant defense response. Mol. Plant-Microbe Interact. 24:183-193.
Mandal, M. K., Chandra-Shekara, A. C., Jeong, R.-D., Yu, K., Zhu, S., Chanda, B., Navarre, D., Kachroo, A., and Kachroo, P. 2012. Oleic acid-dependent modulation of NITRIC OXIDE ASSOCIATED1 protein levels regulates nitric oxide-mediated defense signaling in *Arabidopsis*. Plant Cell 24:1654-1674.
Martin, R. L., Le Boulch, P., Clin, P., Schwarzenberg, A., Yvin, J.-C., Andrivon, D., Nguema-Ona, E., and Val, F. 2020. A comparison of PTI defense profiles induced in *Solanum tuberosum* by PAMP and non-PAMP elicitors shows distinct, elicitor-specific responses. PLoS One 15:e0236633.
Mauri, M., Elli, T., Caviglia, G., Uboldi, G., and Azzi, M. 2017. RAWGraphs: A visualisation platform to create open outputs. Pages 1-5 in: Proceedings of the 12th Biannual Conference on Italian SIGCHI Chapter.
Miya, A., Albert, P., Shinya, T., Desaki, Y., Ichimura, K., Shirasu, K., Narusaka, Y., Kawakami, N., Kaku, H., and Shibuya, N. 2007. CERK1, a LysM receptor kinase, is essential for chitin elicitor signaling in *Arabidopsis*. Proc. Natl. Acad. Sci. U.S.A. 104:19613-19618.
Mundt, C. C. 2014. Durable resistance: A key to sustainable management of pathogens and pests. Infect. Genet. Evol. 27:446-455.
Ngou, B. P. M., Jones, J. D. G., and Ding, P. 2022. Plant immune networks. Trends Plant Sci. 27:255-273.
Nguema-Ona, E., Bannigan, A., Chevalier, L., Baskin, T. I., and Driouich, A. 2007. Disruption of arabinogalactan proteins disorganizes cortical microtubules in the root of *Arabidopsis thaliana*. Plant J. 52: 240-251.
Nühse, T. S., Bottrill, A. R., Jones, A. M. E., and Peck, S. C. 2007. Quantitative phosphoproteomic analysis of plasma membrane proteins reveals regulatory mechanisms of plant innate immune responses. Plant J. 51: 931-940.
Pang, Z., Chong, J., Zhou, G., de Lima Morais, D. A., Chang, L., Barrette, M., Gauthier, C., Jacques, P.-É., Li, S., and Xia, J. 2021. MetaboAnalyst 5.0: Narrowing the gap between raw spectra and functional insights. Nucleic Acids Res. 49:W388-W396.
Piasecka, A., Jedrzejczak-Rey, N., and Bednarek, P. 2015. Secondary metabolites in plant innate immunity: Conserved function of divergent chemicals. New Phytol. 206:948-964.
Přerovská, T., Jindřichová, B., Henke, S., Yvin, J.-C., Ferrieres, V., Burketová, L., Lipovová, P., and Nguema-Ona, E. 2022. Arabinogalactan protein-like proteins from *Ulva lactuca* activate immune responses and plant resistance in an oilseed crop. Front. Plant Sci. 13:893858.
Rojas, C. M., Senthil-Kumar, M., Tzin, V., and Mysore, K. S. 2014. Regulation of primary plant metabolism during plant-pathogen interactions and its contribution to plant defense. Front. Plant Sci. 5:17.
Rojas, C. M., Senthil-Kumar, M., Wang, K., Ryu, C.-M., Kaundal, A., and Mysore, K. S. 2012. Glycolate oxidase modulates reactive oxygen species-mediated signal transduction during nonhost resistance in *Nicotiana benthamiana* and *Arabidopsis*. Plant Cell 24:336-352.
Roux, M., Schwessinger, B., Albrecht, C., Chinchilla, D., Jones, A., Holton, N., Malinovsky, F. G., Tör, M., de Vries, S., and Zipfel, C. 2011. The *Arabidopsis* leucine-rich repeat receptor–like kinases BAK1/SERK3 and BKK1/SERK4 are required for innate immunity to hemibiotrophic and biotrophic pathogens. Plant Cell 23:2440-2455.
Sandroni, M., Liljeroth, E., Mulugeta, T., and Alexandersson, E. 2020. Plant resistance inducers (PRIs): Perspectives for future disease management in the field. CABI Rev. 15:1-10.
Savary, S., Willocquet, L., Pethybridge, S. J., Esker, P., McRoberts, N., and Nelson, A. 2019. The global burden of pathogens and pests on major food crops. Nat. Ecol. Evol. 3:430-439.
Schläpfer, P., Zhang, P., Wang, C., Kim, T., Banf, M., Chae, L., Dreher, K., Chavali, A. K., Nilo-Poyanco, R., Bernard, T., Kahn, D., and Rhee, S. Y. 2017. Genome-wide prediction of metabolic enzymes, pathways, and gene clusters in plants. Plant Physiol. 173:2041-2059.
Schwessinger, B., Roux, M., Kadota, Y., Ntoukakis, V., Sklenar, J., Jones, A., and Zipfel, C. 2011. Phosphorylation-dependent differential regulation of plant growth, cell death, and innate immunity by the regulatory receptor-like kinase BAK1. PLoS Genet. 7:e1002046.
Shibuya, N., Kaku, H., Kuchitsu, K., and Maliarik, M. J. 1993. Identification of a novel high-affinity binding site for *N*-acetylchitooligosaccharide elicitor in the membrane fraction from suspension-cultured rice cells. FEBS Lett. 329:75-78.
Souza, C. de, A., Li, S., Lin, A. Z., Boutrot, F., Grossmann, G., Zipfel, C., and Somerville, S. C. 2017. Cellulose-derived oligomers act as damage-associated molecular patterns and trigger defense-like responses. Plant Physiol. 173:2383-2398.
Sun, Y., Li, L., Macho, A. P., Han, Z., Hu, Z., Zipfel, C., Zhou, J.-M., and Chai, J. 2013. Structural basis for flg22-induced activation of the *Arabidopsis* FLS2-BAK1 immune complex. Science 342:624-628.
Tang, B., Liu, C., Li, Z., Zhang, X., Zhou, S., Wang, G.-L., Chen, X.-L., and Liu, W. 2021. Multilayer regulatory landscape during pattern-triggered immunity in rice. Plant Biotechnol. J. 19:2629-2645.
Thomma, B. P. H. J., Nelissen, I., Eggermont, K., and Broekaert, W. F. 1999. Deficiency in phytoalexin production causes enhanced susceptibility of *Arabidopsis thaliana* to the fungus *Alternaria brassicicola*. Plant J. 19:163-171.
Tsuda, K., Sato, M., Glazebrook, J., Cohen, J. D., and Katagiri, F. 2008. Interplay between MAMP-triggered and SA-mediated defense responses. Plant J. 53:763-775.
Tsugawa, H., Cajka, T., Kind, T., Ma, Y., Higgins, B., Ikeda, K., Kanazawa, M., VanderGheynst, J., Fiehn, O., and Arita, M. 2015. MS-DIAL: Data-independent MS/MS deconvolution for comprehensive metabolome analysis. Nat. Methods 12:523-526.

van Loon, L. C., Rep, M., and Pieterse, C. M. J. 2006. Significance of inducible defense-related proteins in infected plants. Annu. Rev. Phytopathol. 44:135-162.

Wan, Y., Zhang, X.-C., Neece, D., Ramonell, K. M., Clough, S., Kim, S.-y., Stacey, M. G., and Stacey, G. 2008. A LysM receptor-like kinase plays a critical role in chitin signaling and fungal resistance in *Arabidopsis*. Plant Cell 20:471-481.

Wang, Y., Pruitt, R. N., Nürnberger, T., and Wang, Y. 2022. Evasion of plant immunity by microbial pathogens. Nat. Rev. Microbiol. 20:449-464.

Wu, T., Zou, R., Pu, D., Lan, Z., and Zhao, B. 2021. Non-targeted and targeted metabolomics profiling of tea plants (*Camellia sinensis*) in response to its intercropping with Chinese chestnut. BMC Plant Biol. 21:55.

Xin, X.-F., Nomura, K., Aung, K., Velásquez, A. C., Yao, J., Boutrot, F., Chang, J. H., Zipfel, C., and He, S. Y. 2016. Bacteria establish an aqueous living space in plants crucial for virulence. Nature 539:524-529.

Yamada, A., Shibuya, N., Kodama, O., and Akatsuka, T. 1993. Induction of phytoalexin formation in suspension-cultured rice cells by *N*-acetyl-chitooligosaccharides. Biosci. Biotechnol. Biochem. 57:405-409.

Ye, W., Munemasa, S., Shinya, T., Wu, W., Ma, T., Lu, J., Kinoshita, T., Kaku, H., Shibuya, N., and Murata, Y. 2020. Stomatal immunity against fungal invasion comprises not only chitin-induced stomatal closure but also chitosan-induced guard cell death. Proc. Natl. Acad. Sci. U.S.A. 117:20932-20942.

Yu, X., Feng, B., He, P., and Shan, L. 2017. From chaos to harmony: Responses and signaling upon microbial pattern recognition. Annu. Rev. Phytopathol. 55:109-137.

Zahid, A., Jaber, R., Laggoun, F., Lehner, A., Remy-Jouet, I., Pamlard, O., Beaupierre, S., Leprince, J., Follet-Gueye, M.-L., Vicré-Gibouin, M., Latour, X., Richard, V., Guillou, C., Lerouge, P., Driouich, A., and Mollet, J.-C. 2017. Holaphyllamine, a steroid, is able to induce defense responses in *Arabidopsis thaliana* and increases resistance against bacterial infection. Planta 246:1109-1124.

Zaynab, M., Fatima, M., Abbas, S., Sharif, Y., Umair, M., Zafar, M. H., and Bahadar, K. 2018. Role of secondary metabolites in plant defense against pathogens. Microb. Pathog. 124:198-202.

Zeiss, D. R., Steenkamp, P. A., Piater, L. A., and Dubery, I. A. 2021. Altered metabolomic states elicited by Flg22 and FlgII-28 in *Solanum lycopersicum:* Intracellular perturbations and metabolite defenses. BMC Plant Biol. 21:429.

Zipfel, C., Kunze, G., Chinchilla, D., Caniard, A., Jones, J. D. G., Boller, T., and Felix, G. 2006. Perception of the bacterial PAMP EF-Tu by the receptor EFR restricts *Agrobacterium*-mediated transformation. Cell 125:749-760.

Zipfel, C., Robatzek, S., Navarro, L., Oakeley, E. J., Jones, J. D. G., Felix, G., and Boller, T. 2004. Bacterial disease resistance in *Arabidopsis* through flagellin perception. Nature 428:764-767.